ELSEVIER

Chemical Geology 231 (2006) 77–89

CHEMICAL GEOLOGY
INCLUDING
ISOTOPE GEOSCIENCE

www.elsevier.com/locate/chemgeo

Activity coefficients at low dilution of CrO, NiO and CoO in melts in the system $CaO–MgO–Al_2O_3–SiO_2$ at 1400°C: Using the thermodynamic behaviour of transition metal oxides in silicate melts to probe their structure

Hugh St.C. O'Neill *, Andrew J. Berry

Research School of Earth Sciences, Australian National University, Canberra 0200, ACT, Australia

Received 14 June 2005; received in revised form 20 December 2005; accepted 4 January 2006

Abstract

The activity coefficients at low dilution of NiO, CoO and CrO in ~30 silicate melt compositions in the system $CaO–MgO–Al_2O_3–SiO_2$ (CMAS) have been determined with a precision of 3% to 5%, one standard deviation, at 1400 °C by equilibration with the pure metal under controlled oxygen fugacity (Ni and Co) or with Cr_2C_3–graphite–CO. The activity coefficients vary by a factor of two over the range of melt compositions studied, but show no simple correlation with melt chemistry or melt structural descriptors. The variation in activity coefficients with melt composition among NiO, CoO and CrO is nevertheless highly correlated, as it also seems to be with the oxides of other divalent cations of similar ionic radius (e.g., Fe^{2+}, Mg). In the case of NiO and CoO, the correlation is essentially perfect within the precision of the measurements, that is, the ratio $\gamma_{NiO}/\gamma_{CoO}$ is the same for all melt compositions, implying that these two cations occupy a similar distribution of coordination environments in all the investigated CMAS melts. The deviations from a one-to-one correlation of the activity coefficient of CrO with those of NiO and CoO may be due to Cr^{2+} cations occurring in a distribution with more distorted coordination environments, due to the strong Jahn–Teller effect in this cation.

Keywords: Silicate melt; Thermodynamic properties; Activity coefficients; Crystal field theory; Coordination environment; Jahn–Teller effect; Cr; Ni; Co

1. Introduction

It is often pointed out that spectroscopic investigations of silicate glasses or melts can illuminate their thermodynamic as well as their structural properties, but the corollary is equally true: thermodynamic measurements can reveal much about melt structure. In a previous investigation (O'Neill and Eggins, 2002), the activity coefficients of the three divalent transition metal oxide components FeO, NiO and CoO were shown to vary sympathetically with each other as a function of melt composition in melts in the system $CaO–MgO–Al_2O_3–SiO_2$ (CMAS), despite the fact that the divalent transition-metal cations Fe^{2+}, Co^{2+} and Ni^{2+} have rather different electronic configurations.

Here we extend this investigation, by measuring activity coefficients at low dilution (i.e., in the Henry's law region) of CrO. Cr^{2+} has a d^4 electronic configuration,

* Corresponding author. Tel.: +61 2 6125 5159; fax: +61 2 6125 5989.
E-mail address: hugh.oneill@anu.edu.au (H.S.C. O'Neill).

0009-2541/$ - see front matter © 2006 Elsevier B.V. All rights reserved.
doi:10.1016/j.chemgeo.2006.01.004

giving rise to strong Jahn–Teller effects in both tetrahedral and octahedral crystal fields. In silicate melts, in which the geometrical constraints from long-range order imposed by crystal structure are absent, cations are expected to occupy a variety of coordination environments, which may be thought of as forming a distribution. For a cation with a well-defined preference for a particular coordination geometry, such a distribution would be unimodal, characterised by a mean or preferred coordination environment, with a standard deviation, and other statistical properties that define a distribution such as skewness and kurtosis. But in some cases the distribution may be bimodal, for example if the cation has a preference for both octahedrally and tetrahedrally coordinated environments. Even more complex distributions are also possible. The distribution will be the product of the cation's electronic structure interacting with the melt structure that derives from the major-element chemistry of the melt, pressure and temperature. The distribution of coordination environments around Jahn–Teller-active cations may be expected to differ from cations that prefer a high-symmetry coordination geometry, making it probable that the thermodynamic properties of such cations, of which Cr^{2+} is an example, might respond differently to varying melt chemistry, compared to cations in which the Jahn–Teller effect is less important or absent.

In O'Neill and Eggins (2002) 18 CMAS compositions were investigated, but for this study we have increased the number of melt compositions to 31, reporting new measurements for Co and Ni, not only for the 13 new compositions, but also replicating the original 18 compositions, to demonstrate consistency with the earlier study. In the same spirit, we have also reanalysed the Ni and Co experiments from the earlier study using the analytical protocols adopted for this study.

1.1. Thermodynamic background

For elements whose oxides are easily reduced to the metal (i.e., Ni and Co), activity coefficients in silicate melts ($\gamma^{melt}_{MO_{x/2}}$) may be measured using the redox reaction:

$$\underset{\text{metal}}{M} + x/4\,O_2 = \underset{\text{silicate melt}}{MO_{x/2}} \quad (1)$$

Hence at equilibrium:

$$\ln\gamma^{\text{sil melt}}_{MO_{x/2}} = \frac{-\Delta_f G^o_{(MO_{x/2})}}{RT} - \ln X^{\text{sil melt}}_{MO_{x/2}} + \frac{x}{4}\ln fO_2 + \ln a^{\text{metal}}_M \quad (2)$$

If the metal M is pure, $\ln a^{\text{metal}}_M = 0$, while $\Delta_f G^o_{(MO_{x/2})}$ is a constant at constant T and P. Hence the activity coefficient is directly related to the metal's solubility (given by $X^{\text{sil melt}}_{MO_{x/2}}$), if fO_2 is imposed, as may be done using the usual gas-mixing methods, e.g., CO–CO_2 mixtures in O'Neill and Eggins (2002). However, the range of fO_2 required for equilibrium with Cr metal is too low to be accessed accurately using CO–CO_2 or CO_2–H_2 gas mixes at 1400 °C (e.g., Holzheid and O'Neill, 1995), so instead we have used the reaction:

$$\underset{\text{carbide}}{2/3\,Cr_3C_2} + \underset{\text{gas}}{CO} = \underset{\text{silicate melt}}{CrO} + \underset{\text{graphite}}{7/3C} \quad (3)$$

Experimentally, this reaction can be implemented very conveniently by using the necessary graphite as the capsule material with the atmosphere of CO provided in the usual way by flowing this gas through the furnace. Although, unlike for the Ni, Co and Fe experiments, there is only limited flexibility in setting the experimental conditions (practically, the CO could be diluted with Ar to access even lower fO_2), it is a matter of serendipity that the amount of CrO dissolved in a silicate melt under the condition of pure CO happens to be just about the optimum level of ~3000 ppm that was selected previously by O'Neill and Eggins (2002) for their Ni and Co experiments. The oxygen fugacity of the graphite–CO equilibrium at 1400 °C and 1 bar is $10^{-16.1}$ bars (calculated from the thermodynamic data in Chase, 1998), which is more than six order of magnitude lower than the $10^{-9.7}$ bars of the Fe–"FeO" equilibrium (iron–wüstite) at the same conditions. Under these extremely reducing conditions all Cr dissolves in the melt as Cr^{2+} (Berry and O'Neill, 2004; Berry et al., submitted for publication).

Previously, Pretorius and Muan (1992) measured the activities of CrO in CaO–SiO_2 and CaO–Al_2O_3–SiO_2 melts at 1500 °C by equilibration with Pt–Cr alloys at oxygen fugacities imposed by CO_2–H_2 gas mixtures where Cr^{3+} was low, although not completely negligible. The precision of these measurements is expected to be lower than those described here, due to the uncertainty in the determination of both $Cr^{2+}/\sum Cr$ and the composition of the Pt–Cr alloys, and to the lack of a suitable chemically inert crucible. Xiao et al. (2002) undertook a similar study of CaO–SiO_2 melts at 1600 °C using Cr–Ag alloys. Both these sets of measurements are not easy to compare with the results reported here, because at the much higher concentrations of dissolved Cr, the CrO concentrations are not in the Henry's law region.

2. Experimental

2.1. Sample equilibration

Silicate melt compositions were prepared from reagent grade MgO and Al_2O_3, both dried before weighing at 1100 °C, fine-grained SiO_2 prepared from $SiO_2{\cdot}nH_2O$ ("silicic acid") by dehydrating at 1100 °C, and $CaCO_3$, dried at ~300 °C. Mixtures were homogenised by grinding under acetone in an agate mortar, pressed into pellets and decarbonated by heating slowly to ~1100 °C, followed by regrinding.

The compositions were run in five sets of five to seven samples: the sets "AD6", "CMAS7" and "CAS/MAS eutectics" were used previously in O'Neill and Eggins (2002), in which reference a description of their significance is given. The TiO_2-containing composition "AD+TiO_2" from the "AD6" set was not used in this study, because much of the Ti would be Ti^{3+} at the very low fO_2 of the Cr experiments, but Ti^{4+} in the Ni and Co experiments (Schreiber, 1977). Twelve of the new compositions introduced in this study have relatively low liquidus temperatures, selected with guidance from the phase relations determined at atmospheric pressure by Osborn et al. (1954) and Longhi (1987) and are designated Os1-6 and L1-6 respectively (e.g., Table 1). The set "L6" from Longhi (1987, p.294) comprise: L1, peritectic at 1315 °C; L2, co-planarity at 1240 °C; L3, co-planarity at 1229 °C; L4, co-planarity at 1215 °C; L6, eutectic at 1207 °C; the intended L5 was made up to the wrong composition due to a transcription error and this composition is designated L5x. The set "OS6" from Osborn et al. (1954) was selected to expand the range of low SiO_2 compositions investigated (five out of the six have $SiO_2<50$ wt.%). An additional composition in the subsystem CaO–Al_2O_3–SiO_2 (CAS) is the eutectic between SiO_2, α-$CaSiO_3$ and anorthite at 1170 °C, from Rankin and Wright (1915), called CAS5.

The Ni and Co experiments were carried out as described in O'Neill and Eggins (2002), except that for Ni a gas mixture of 60% CO, corresponding to fO_2 of $10^{-8.96}$ bars, was used, rather than the $fO_2=10^{-9.60}$ bars used in the previous study, while for Co, a mix of 96% CO, giving fO_2 of $10^{-11.37}$ bars, was used compared to $10^{-11.62}$ bars previously. The effect of these increases in fO_2 is to elevate the amounts of Ni and Co in the equilibrated melts, thus increasing accuracy slightly. In addition, the flow rate of gas was approximately doubled to 200 standard cubic centimetres per minute (SCCM), giving a linear flux through the furnace tube (4.3 cm diameter) of 0.23 cm/s; this increased flow rate should result in an improved control of fO_2. In order to optimise the precision in fO_2 control, the mass flow controllers were set to the desired flow rates and the five Ni or Co experiments were then done one after the other without adjusting the mass flow controllers. In this way, we believe that a precision of about ±0.01 in log fO_2 may be achieved for a short series of runs as reported here.

Table 1
Major element compositions from Ni and Co solubility experiments, renormalized to 100% on a Ni-, Co-free basis

Composition	SiO_2	Al_2O_3	MgO	CaO	$\sum N_{ZO_{y/2}}^{sil\ melt}$ [a]	NBO/T	Optical basicity
AD6							
ADeu	50.2	15.6	10.9	23.3	1.827	0.933	0.605
AD+Fo	49.0	13.2	17.7	20.1	1.872	1.243	0.609
AD+En	54.0	9.8	21.6	14.7	1.887	1.286	0.595
AD+Wo	51.2	6.5	4.6	37.9	1.768	1.482	0.632
AD+Qz	65.5	10.7	7.5	16.3	1.777	0.572	0.562
CMAS7							
CMASA	55.5	15.9	12.8	15.8	1.835	0.717	0.582
CMASB	56.1	14.4	21.1	8.5	1.889	0.878	0.577
CMASC	56.8	6.8	20.6	15.8	1.871	1.346	0.592
CMASD	47.2	21.7	18.9	12.2	1.897	0.782	0.594
CMASE	49.1	10.5	19.9	20.5	1.882	1.478	0.614
CMASF	61.7	6.2	14.2	18.0	1.820	1.066	0.581
CMASG	59.2	12.8	2.6	25.4	1.754	0.634	0.585
CAS/MAS eutectics							
MAS1	61.0	17.9	21.0	0.1	1.889	0.508	0.552
MAS2	50.8	23.2	26.0	0.1	1.945	0.644	0.572
CAS1	42.7	19.9	0.0	37.5	1.768	0.860	0.636
CAS2	42.0	12.0	0.0	46.0	1.754	1.504	0.662
CAS3	69.8	19.8	0.1	10.4	1.736	−0.011	0.534
CAS4	54.1	12.8	0.0	33.1	1.742	0.807	0.607
CAS5	61.2	15.1	0.0	23.7	1.738	0.418	0.574
L6							
L1	62.7	7.6	14.1	15.6	1.821	0.928	0.574
L2	50.0	14.1	5.7	30.2	1.789	0.977	0.615
L3	62.5	18.2	9.5	9.9	1.807	0.334	0.555
L4	62.3	15.0	5.3	17.4	1.773	0.443	0.566
L5x	67.6	17.6	9.3	5.5	1.799	0.212	0.539
L6	62.1	15.3	8.8	13.8	1.798	0.471	0.563
Os6							
Os1	47.3	10.4	9.4	33.0	1.811	1.452	0.633
Os2	50.8	15.4	4.2	29.6	1.780	0.838	0.610
Os3	47.7	15.3	14.4	22.6	1.854	1.115	0.613
Os4	45.1	15.3	11.3	28.3	1.836	1.208	0.626
Os5	42.1	20.5	9.5	28.0	1.836	0.968	0.627
Os6	49.5	20.4	15.4	14.7	1.868	0.725	0.592

[a] Number of moles of CaO, MgO, $AlO_{1.5}$ and SiO_2 in 100 g of melt.

The Cr experiments were done as follows. Discs 24 mm diameter by 12 mm thick were machined from high purity graphite. Five to seven holes for the samples, 4.3 mm in diameter and ~10 mm deep, were drilled around the outer part of the disc (see Fig. 1a). These

sample holes were filled in a sandwich arrangement with ~100 mg Cr_3C_2 (99.7% stated purity, from Strem Chemicals) at top and bottom, and ~150 mg of the silicate melt composition in the middle; the filling was topped with a graphite lid (2 mm thick). The graphite disc was suspended in the furnace using alumina ceramics only and no metal wire (Fig. 1b), because all likely metals react with the carbon available from the CO gas at graphite saturation. The arrangement allowed drop quenching into water in the usual way (Fig. 1c and d).

2.2. Electron microprobe analysis

Runs were analysed using a Cameca SX100 electron microprobe in the wavelength dispersive (WDS) mode. Column conditions were an accelerating voltage of 25 kV, and beam currents of 40 nA for Ni and Cr samples, and 20 nA for Co, with the beam defocused to 10 μm. Standards were synthetic MgO for Mg, synthetic $CaAlO_2$ for Al, natural wollastonite for Ca and Si, and Cr, Ni, or Co metals for these elements. Counting times were 20 s on peak and 10 s on background either side of the peak for the major elements, and 60 s on peak, 30 s background either side for Ni, Co and Cr. Twelve spot analyses were performed on each sample. Data were reduced using the phi–rho–Z correction procedure as implemented in the Cameca software. The Ni and Co runs from O'Neill and Eggins (2002) were reanalysed for both major elements and Co and Ni using the above conditions as a check on consistency with this earlier experimental campaign. Note that the electron microprobe data reported in O'Neill and Eggins (2002) was reduced using the ZAF procedure from Ware (1981).

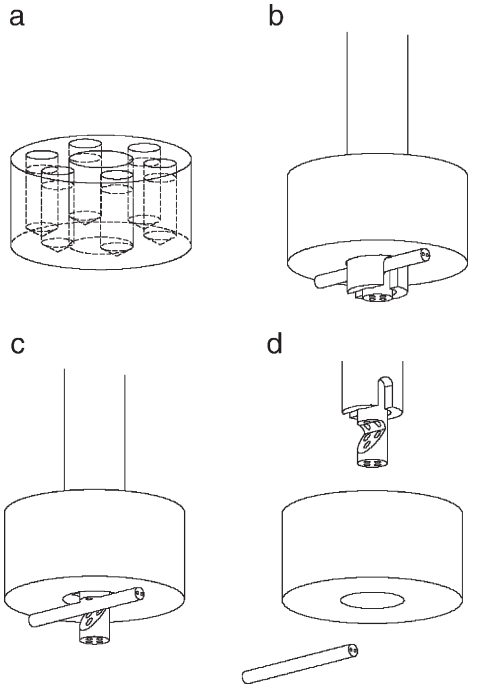

Fig. 1. The wireless rapid-quench apparatus used for the CrO experiments. a) shows the graphite disc with six holes to take six samples. The disc is mounted on an alumina tube passing through its seventh, middle hole, as shown in b); it is secured with a piece of thermocouple ceramic held in place by a notch cut into an alumina rod that is inserted through the tube, the tube and rod both being held in place at the top of the furnace, the rod by a compressed O-ring. Pushing the rod downwards releases the piece of thermocouple ceramic from its notch (c), allowing the graphite disc to fall (d).

3. Results

3.1. Results: precision and reproducibility of the Ni and Co data

Electron microprobe analytical results for major elements averaged from both the Ni and Co experiments are given in Table 1; for the compositional sets AD6, CMAS7 and CAS/MAS eutectics, the averages include the new analyses of the experiments of O'Neill and Eggins (2002), and are thus of 48 individual analyses (12 on each of four samples, two Ni and two Co). For the new compositions comprising the L6 and Os6 sets, the averages are from 24 individual analyses (12 each on the Ni and Co samples). For the AD6, CMAS7 and CAS/MAS sets, the major-element analyses show some small systematic differences with those given in O'Neill and Eggins (2002), which were obtained on our old Cameca Camebax electron microprobe in the energy-dispersive (EDS) mode.

The Ni and Co analyses are reported in Table 2, together with the standard deviations calculated from the 12 individual analyses (all uncertainties in this paper are given as one standard deviation of the mean). The reanalyses of the runs from O'Neill and Eggins (2002) give Ni contents in complete agreement with the earlier reported analyses, which may be demonstrated quantitatively by regression of the new analyses against the old, weighting the data according to the observed uncertainties:

$$[\mathrm{Ni}]_{\mathrm{new}} = [\mathrm{Ni}]_{\mathrm{old}} \times 1.002(\pm 0.009), \quad \chi^2_{\mathrm{v}} = 0.80.$$

The same regression for the Co data gives:

$$[\mathrm{Co}]_{\mathrm{new}} = [\mathrm{Co}]_{\mathrm{old}} \times 1.029(\pm 0.008), \quad \chi^2_{\mathrm{v}} = 1.97$$

i.e., the new Co analyses are on average 3% higher than those reported in O'Neill and Eggins (2002). These

Table 2
Ni and Co solubilities (in ppm) in equilibrium with pure Ni or Co at 1400 °C

Composition	Ni (O'N and E, 2002)[a]	σ(Ni) (O'N and E, 2002)	Ni (This work)[b]	σ(Ni) (This work)	Co (O'N and E, 2002)[c]	σ(Co) (O'N and E, 2002)	Co (This work)[d]	σ(Co) (This work)
AD6								
ADeu	1841	38	3386	70	2928	90	3450	44
AD+Fo	1827	51	3501	40	3078	88	3486	70
AD+En	2154	16	3681	62	3716	53	3985	66
AD+Wo	2232	32	4098	52	3478	139	4134	41
AD+Qz	1655	25	3074	87	2932	50		
CMAS7								
CMASA	1927	63			3248	29	3670	93
CMASB	2301	74	4117	33	3912	49	4347	37
CMASC	2446	44	4364	48	3983	52	4628	21
CMASD	1852	60	3596	34	3093	32	3609	68
CMASE	1842	25	3442	25	3139	51	3644	43
CMASF	2335	54	4294	49	4106	72	4450	97
CMASG	1894	85	3368	52	3258	39	3633	45
CAS/MAS eutectics								
MAS1	2478	78			4278	110	4944	43
MAS2	2684	28	4927	101	4439	88	5270	106
CAS1	1293	34	2598	43	1979	32	2518	51
CAS2	1287	29	2562	29	2067	37	2461	53
CAS3	1112	51	2261	100	2333	39	2312	54
CAS4	2009	67	3644	44	3298	109	3931	36
CAS5			3160	75			3077	35
L6								
L1			3871	61			4433	29
L2			–				3413	25
L3			3226	109			3238	37
L4			2860	49			2977	39
L5x			2545	29			2636	115
L6			2777	23			3295	65
Os6								
Os1			3056	49			3466	57
Os2			3060	34			3372	78
Os3			3174	53			3320	51
Os4			2867	105			3061	71
Os5			2457	103			2508	43
Os6			3284	30			3586	88

[a] $fO_2 = 10^{-9.60}$ bars; [b] $fO_2 = 10^{-8.60}$ bars; [c] $fO_2 = 10^{-11.62}$ bars; [d] $fO_2 = 10^{-11.37}$ bars.

experiments were also analysed previously using laser-ablation ICP-MS (O'Neill and Eggins, 2002), with results that were 3±1% higher for Ni and 1±1% for Co, compared to the old set of EMP analyses. The general conclusion is that systematic errors at about the ±3% level may be expected between analytical campaigns.

For the 18 compositions in the three sets AD6, CMAS7 and CAS/MAS, the new experiments ("this work" in Table 2) may similarly be compared to those previously reported in O'Neill and Eggins (2002), by regressing the one against the other. For the O'Neill and Eggins (2002) experiments, we have used the new analyses (also Table 2):

$$[\mathrm{Ni}]_{\text{this work}} = 1.843(\pm 0.012)[\mathrm{Ni}]_{\text{O'N\&E}}, \quad \chi^2_\nu = 3.1$$

The difference in fO_2 between the Ni experiments of this work versus that used in O'Neill and Eggins (2002), i.e., log fO_2 (bars) = −8.96 versus −9.60, implies that the Ni solubilities of this work should be a factor of 2.09 higher, rather than the 1.84 returned by the regression; there is therefore an apparent systematic error in log fO_2 of 0.11 log-bar units between the two sets of

experiments. For Co, the regression of the two data sets gives:

$$[\mathrm{Co}]_{\text{this work}} = 1.139(\pm 0.006)[\mathrm{Co}]_{\text{O'N\&E}}, \quad \chi^2_{\nu} = 4.4$$

Here the increase in log fO_2 from −11.62 to −11.37 should have caused an increase in Co solubilities of 1.33 rather than the factor of 1.14 that is observed, implying a systematic discrepancy in log fO_2 of 0.14 log-bar units, that is, very similar to that between the two sets of Ni experiments. The different experimental campaigns were carried out in different furnaces, with different sets of mass flow controllers, several years apart; we conclude that under such circumstances, systematic errors of the order of 0.1 in log fO_2 are evidently possible with our experimental set-up.

For both of these comparison regressions, the values of the χ^2_{ν} statistic are about double those expected, using the observed analytical uncertainties reported in Table 2, which are often only ~1%, but vary up to ~3%. The high values of χ^2_{ν} imply that the uncertainties of ~1% are unrealistically optimistic, perhaps due to the neglect of non-random analytical errors or to local fluctuations in fO_2, and that using an uncertainty of 3% for all data would be more appropriate, as in O'Neill and Eggins (2002); this also fits with the conclusion reached above that different analytical campaigns can result in systematic errors of about this magnitude. This level of uncertainty is considerably less than that due to the level of systematic error caused by ~0.1 log-bar unit in fO_2 between experimental campaigns noted above. It is important to bear in mind when comparing the results between studies (as done for Ni and Co in O'Neill and Eggins, 2002) that if the usual level of experimental uncertainty in fO_2 control is indeed about ±0.1 log-bar unit, as seems reasonable, this would obscure the subtle relationships between activity–composition relations among NiO, CoO and CrO that we discuss below.

3.2. Cr solubilities in equilibrium with Cr_2C_3 + graphite at p(CO) = 1 bar

The major elements analyses are reported along with the Cr concentrations in Table 3. Under extremely reducing conditions SiO_2 can become volatile in one-atmosphere gas-mixing experiments, but in the present experimental arrangement this was ameliorated considerably by using the graphite lid, and by running experiments for 3–4 days only, with the gas flow rate of CO through the furnace lowered to 15 SCCM. The results show that the loss of SiO_2 was limited to less than about 2%, relative, which is almost completely negligible. Shorter run durations evinced considerable heterogeneity in Cr contents dissolved in the glasses (including micronuggets), while an experiment with the substantially longer duration of 18 days, although beautifully homogenous, showed excessive losses of SiO_2 of ~10% in most compositions.

3.3. Activity coefficients

For each composition, the Ni, Co and Cr concentrations were converted to mole fractions according to the relationship:

$$(X^{\text{sil melt}}_{MO_2}) = \frac{[M] \times 10^{-4}/A_r}{[M] \times 10^{-4}/A_r + \sum N^{\text{sil melt}}_{ZO_{y/2}}} \tag{4}$$

where $[M]$ is the concentration of Ni, Co or Cr in ppm by weight, A_r is the atomic weight of these elements, and $\sum N^{\text{sil melt}}_{ZO_{y/2}}$ is the total number of moles of the major-element oxides on a single cation basis (i. e., $N^{\text{sil melt}}_{SiO_2} + N^{\text{sil melt}}_{AlO_{1.5}} + N^{\text{sil melt}}_{CaO} + N^{\text{sil melt}}_{MgO}$) in 100 g of M-free melt. The values of $\sum N^{\text{sil melt}}_{ZO_{y/2}}$ for each melt composition are given in Table 1. The activity coefficients $\gamma^{\text{sil melt}}_{MO}$ were then calculated (Eq. (1)), using $\Delta_f G^{o}_{(NiO,l)}/RT = -5.67$ and $\Delta_f G^{o}_{(CoO,l)}/RT = -7.57$ (O'Neill and Eggins, 2002). Note that the standard state is the pure liquid oxide at the temperature of interest. Calculated activity coefficients are given in Table 4.

For CrO, thermodynamic data for the pure oxide are poorly known, because solid CrO is unstable relative to $Cr + Cr_2O_3$ or $Cr + Cr_3O_4$ below the liquidus of the Cr–O system (Toker et al., 1991). The thermodynamic properties of Cr_3C_2 are even more poorly known at the temperature of this study (Kleykamp, 2001). Accordingly, we calculate relative activity coefficients (designated here γ^{*}_{CrO}), adopting one of the compositions, namely anorthite–diopside eutectic (ADeu), arbitrarily as a reference state (i.e., $\gamma^{*}_{CrO} = \gamma_{CrO}/\gamma^{ADeu}_{CrO}$). These relative activity coefficients are also given in Table 4.

3.4. Colour of the glasses

Apart from changes in intensity due to different amounts of dissolved Ni, Co, or Cr, the colour of the quenched glasses in this study does not vary perceptibly among the different compositions. (The colour is brown for Ni, royal blue for Co and Cr; the Fe^{2+} glasses from O'Neill and Eggins (2002) have a light turquoise blue colour). However, this is not necessarily a good indication of a constant coordination distribution because of the different magnitude of extinction coefficients for cations in octahedral and tetrahedral coordination.

Table 3
Major element compositions (renormalized to 100 wt.% on a Cr-free basis) and Cr solubilities in equilibrium with Cr_3C_2+graphite at 1400 °C and p(CO)=1 bar

Composition	SiO_2	Al_2O_3	MgO	CaO	Cr (ppm)	σ(Cr/ppm)
AD6 (88 h)						
ADeu	49.1	16.0	11.1	23.9	2924	22
AD+Fo	48.6	13.5	17.8	20.2	2739	53
AD+En	53.1	10.3	21.1	15.5	3656	28
AD+Wo	50.3	6.8	4.5	38.4	3473	86
AD+Qz	65.8	10.8	7.3	16.1	2913	46
CMAS7 (72 h)						
CMASA	55.5	15.9	12.7	15.9	4274	143
CMASB	55.1	14.7	21.3	8.9	4961	89
CMASC	56.4	7.0	20.8	15.7	4697	55
CMASD	47.3	22.2	18.8	11.7	3283	94
CMASE	49.6	10.9	19.9	19.7	2906	21
CMASF	61.5	6.4	14.5	17.7	4605	59
CMASG	58.8	13.3	2.5	25.4	3271	139
CAS/MAS eutectics (76 h)						
MAS1	60.3	18.3	21.3	0.1	4028	19
MAS2	50.5	23.5	26.0	0.0	5094	70
CAS1	43.0	20.4	0.0	36.7	1905	18
CAS2	42.8	12.4	0.0	44.8	1712	17
CAS3	70.5	19.4	0.0	10.0	1424	128
CAS4	54.5	13.2	0.0	32.3	3180	59
L6 (96 h)						
L1	61.6	8.0	14.7	15.7	4127	76
L2	48.4	14.5	5.9	31.2	2461	106
L3	61.0	18.6	10.0	10.4	2786	81
L4	61.4	15.2	5.2	18.1	2615	23
L5x	67.4	17.7	9.3	5.5	1176	66
L6	60.7	15.8	9.2	14.3	2559	44
Os6 (72 h)						
Os1	46.6	10.3	9.1	33.9	2489	30
Os2	49.9	15.4	4.2	30.5	2980	64
Os3	47.2	15.4	14.3	23.1	2673	69
Os4	44.2	15.4	11.3	29.1	2148	58
Os5	41.4	20.4	9.1	29.1	1891	52
Os6	48.5	20.6	15.5	15.4	3031	21

Moreover, it has been shown by a high-temperature EXAFS study on Ni^{2+} in $Na_2Si_2O_5$ (Farges and Brown, 1996) and by optical spectroscopy of Ni^{2+} and Co^{2+} in a haplogranitic composition (Keppler and Bagdassarov, 1999) that the coordination environment changes across the glass transition, so that the colours of quenched glasses do not necessarily reflect coordination environments in the melt anyway. The optical spectra of Ni^{2+} differ considerably in glasses of compositions other than the relatively restricted range of CMAS compositions considered here, that is, in borate, phosphate and alkali-rich silicate glasses (Galoisy and Calas, 1993; Calas et al., 2002).

4. Discussion

4.1. Correlations between activity coefficients

There is a remarkable correlation between the ways that γ_{NiO}, γ_{CoO} and γ^*_{CrO} vary as a function of composition, as shown in Fig. 2.

Table 4
Activity coefficients of NiO, CoO and relative activity coefficients of CrO in silicate melts

Composition	γ_{NiO}	γ_{CoO}	γ^*_{CrO}
AD6			
ADeu	3.05	1.26	1.00
AD+Fo	3.02	1.27	1.09
AD+En	2.90	1.12	0.83
AD+Wo	2.44	1.02	0.82
AD+Qz	3.27	1.43	0.98
CMAS7			
CMASA	2.85[a]	1.19	0.69
CMASB	2.60	1.03	0.61
CMASC	2.43	0.96	0.64
CMASD	2.98	1.25	0.93
CMASE	3.09	1.23	1.04
CMASF	2.40	0.97	0.63
CMASG	2.95	1.15	0.86
CAS/MAS eutectics			
MAS1	2.33[a]	0.91	0.75
MAS2	2.24	0.88	0.61
CAS1	3.85	1.66	1.48
CAS2	3.87	1.69	1.64
CAS3	4.34	1.78	1.95
CAS4	2.70	1.05	0.88
CAS5	3.11	1.34	–
L6			
L1	2.66	0.98	0.71
L2		1.24	1.16
L3	3.17	1.32	1.04
L4	3.50	1.41	1.08
L5x	4.00	1.62	2.44
L6	3.66	1.29	1.13
Os6			
Os1	3.35	1.24	1.16
Os2	3.29	1.25	0.96
Os3	3.30	1.33	1.11
Os4	3.62	1.42	1.37
Os5	4.22	1.74	1.55
Os6	3.22	1.24	0.99

For NiO and CoO, the standard state is the pure liquid at the temperature of interest (1400 °C); for CrO, it is CrO dissolved in the anorthite–diopside eutectic composition (ADeu), i.e., $\gamma^*_{CrO}=\gamma_{CrO}/\gamma^{ADeu}_{CrO}$.

[a]Calculated from the results of O'Neill and Eggins (2002), including an adjustment for the systematic discrepancy between that study and this as described in the text.

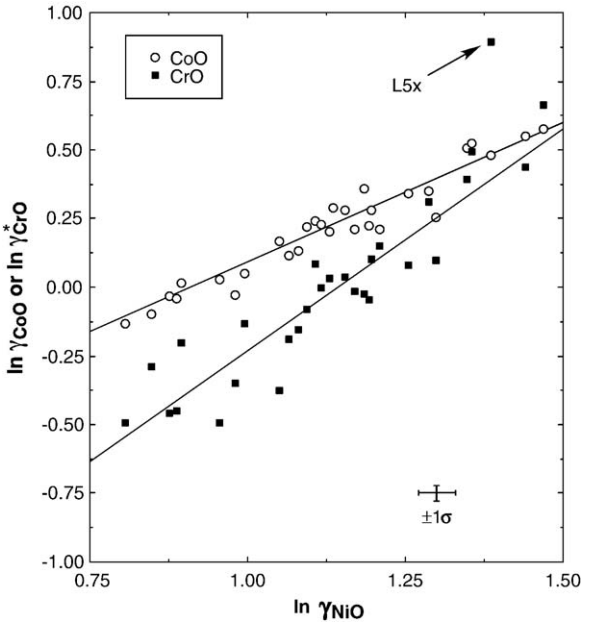

Fig. 2. Linear correlations between ln γ_{CoO} and ln γ_{NiO} and between ln γ^*_{CrO} and ln γ_{NiO} for the CMAS melts used in this study. The slope of the correlation between ln γ_{CoO} and ln γ_{NiO} is constrained to be unity.

For NiO and CoO, regressing the one set of data against the other gives:

$$\ln\gamma_{CoO} = 1.05(\pm0.05)\ln\gamma_{NiO} - 0.974(\pm0.052)$$

With both the Ni and Co data sets weighted at ±3%, which is our estimated analytical uncertainty, the value of the reduced chi-squared statistic (χ^2_ν) is 1.39 (n=30), indicating, statistically, a perfect fit. The slope of the correlation is within error of unity; fixing the slope at 1.0, the regression gives:

$$\ln\gamma_{CoO} = \ln\gamma_{NiO} - 0.912(\pm0.008), \quad \chi^2_\nu = 1.47.$$

The correlation of ln γ_{FeO} with ln γ_{NiO} (O'Neill and Eggins, 2002) is generally similar to that between ln γ_{CoO} and ln γ_{NiO}, but with a slope that is perhaps slightly greater than unity — a best-fit for the 18 compositions studied by O'Neill and Eggins (2002) returns a slope of 1.1±0.1.

By contrast, for CrO, the empirical correlation with NiO clearly indicates a slope greater than unity, as shown in Fig. 2. The regression gives:

$$\ln\gamma^*_{CrO} = 1.61(\pm0.06)\ln\gamma_{NiO} - 1.84(\pm0.07)$$

with χ^2_ν is 4.0 (n=28) with both sets of data weighted at ±3%; the result for the composition L5x is obviously anomalous (Fig. 2) and was omitted from this regression. The rather high value of χ^2_ν reflects the fact that the correlation is not as exact as that between Ni and Co; although this could be due to greater experimental uncertainty in the CrO experiments, the only identifiable contribution to extra uncertainty is that the equilibrium controlling the solubility of CrO (reaction (3)) is dependent on the total pressure of the gas flowing through the furnace, which is likely to fluctuate by ±2% due to meteorological conditions, whereas fO_2 in the Ni and Co experiments is controlled by the ratio CO/CO_2 and is thus independent of ambient pressure. Hence, we suspect that the scatter in ln γ^*_{CrO} versus ln γ_{NiO} is real, that is, it depends on melt structure and chemistry. This is also indicated by the fact that the slope of the correlation is not unity, unlike that found for the Ni vs. Co correlation.

A good correlation between γ_{FeO} and γ_{MgO} was found by Doyle and Naldrett (1986), who showed that in pseudo-ternary melts of the type "Matrix"–MgO–FeO, the activity of FeO was given by:

$$a_{FeO} = a^{Mg-free}_{FeO} \times X_{FeO}/(X_{MgO} + X_{FeO})$$

This implies that for a given "Matrix" composition, the ratio $\gamma_{FeO}/\gamma_{MgO}$ is constant as FeO replaces MgO. Although this compositional constraint is rather restrictive, Toplis (2005) has recently shown that the ratio $\gamma_{FeO}/\gamma_{MgO}$ remains almost constant (in detail, there is a small dependence on silica content as well as concentration of alkalis), from fitting the large body of experimental data that exists for the partitioning of Fe^{2+} and Mg between olivine and silicate melt to a thermodynamic model. This is despite the fact that MgO is obviously a major component of melts in equilibrium with olivine, such that its activity coefficient may be expected to depend on its own concentration. The correlation between γ_{FeO} and γ_{MgO} demonstrated by Toplis encompasses melts with alkalis (Na and K) and Ti, and therefore in one way covers a wider range of melt compositions than addressed in this study, although, conversely, it is necessarily limited to compositions with low activity of silica that are in equilibrium with olivine, whereas the experiments reported here include melt compositions with high silica activity that are nearly quartz-saturated.

Doyle and Naldrett (1987) also demonstrated a similar constancy of the ratio $\gamma_{NiO}/\gamma_{MgO}$ in experiments in systems of the type "Matrix"–MgO–NiO as they had previously with $\gamma_{FeO}/\gamma_{MgO}$ in "Matrix"–MgO–FeO. Taken all together, these correlations establish that Mg should be included along with Fe, Ni, Co and Cr among the group of divalent cations showing similar thermodynamic behaviour in silicate melts.

As pointed out by O'Neill and Eggins (2002), the actual values of γ_{FeO}, γ_{NiO} or γ_{CoO} do not correlate with any simple compositional parameter or melt structural descriptor. A plot of ln γ_{NiO} versus X_{SiO_2} (Fig. 3) shows a rough parabolic dependence, with a minimum around X_{SiO_2}=0.55. The lack of any correlation with the two melt structural descriptors NBO/T (the ratio of non-bridging oxygens to tetrahedral cations, see Mysen, 1990) and optical basicity (Duffy, 1993) is shown in Fig. 4a,b. (Values of both NBO/T and optical basicity are given in Table 1 for the melt compositions used in this study). We have explored a number of other possibilities such as CaO/SiO_2, $(CaO+MgO)/SiO_2$, $SiO_2+Al_2O_3$, etc. without finding any more convincing a correlation. This lack of any simple relationship is further emphasised by fitting the data to the subregular solution model for a trace-element component at infinite dilution (see O'Neill and Eggins, 2002):

$$\ln\gamma_{MO} = \sum_{j=1}^{4}\sum_{k=1}^{j} a_{jk}X_jX_k \qquad (5)$$

The results of these fits are given in Table 5.

In discussing the correlations between the activity coefficients of the FeO, CoO, NiO and MgO in silicate melts, we have emphasised that the ratios of the activity coefficients of two of these components are more-or-less constant in a given melt composition. This is indeed a fair description of their first-order behaviour. In detail, however, there do appear to be some minor but systematic variations in these activity coefficient ratios. From their results, O'Neill and Eggins (2002) suggested that the ratios $\gamma_{FeO}/\gamma_{NiO}$ and, less certainly, $\gamma_{CoO}/\gamma_{NiO}$ correlated with X_{SiO_2}; here, however, we find that with the expanded set of melt compositions used in this study, this latter correlation disappears (i.e., $\gamma_{CoO}/\gamma_{NiO}$ is constant to within the precision of our measurements). There is a small variation in $\gamma_{FeO}/\gamma_{MgO}$ found by Toplis (2005), which correlates well with X_{SiO_2}. In the present results, we observe a correlation, admittedly somewhat weak, between $\gamma^*_{CrO}/\gamma_{NiO}$ and X_{SiO_2} (Fig. 5a), if the two data at highest X_{SiO_2} (CAS3 and L5x) are omitted. The best fit from least-squares regression without these two data gives:

$$\ln\gamma^*_{CrO}/\gamma_{NiO} = -0.62-1.12X_{SiO_2}$$

with χ^2_v=4.4 (n=27), weighting the data for Cr at ±5% and Ni at ±3%. This fit is shown in Fig. 5a. The conclusion is that there is indeed a general tendency for the ratio of two divalent metal oxide activity coefficients

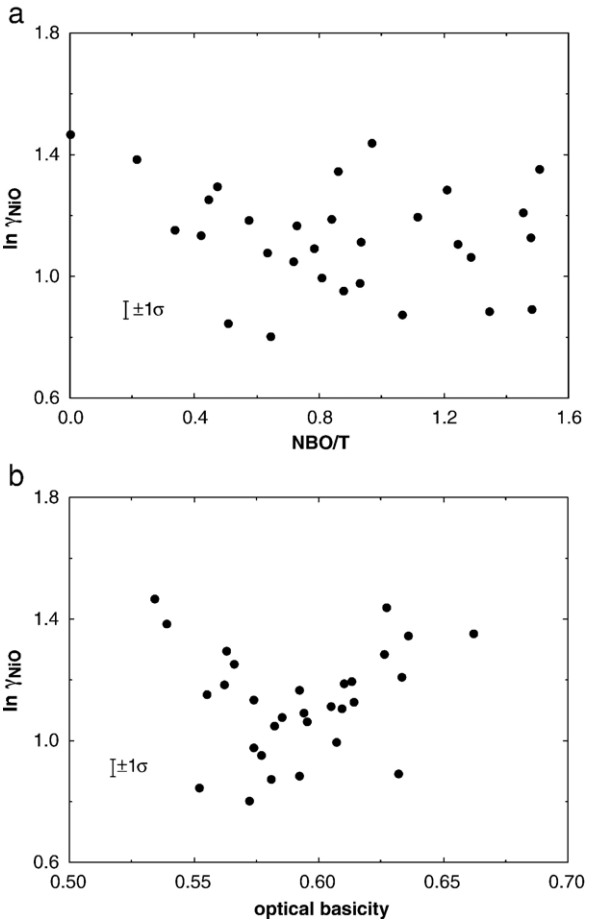

Fig. 4. ln γ_{NiO} versus (a) NBO/T, the ratio of non-bridging oxygens to tetrahedral cations; and (b) optical basicity. In neither plot is a correlation observable.

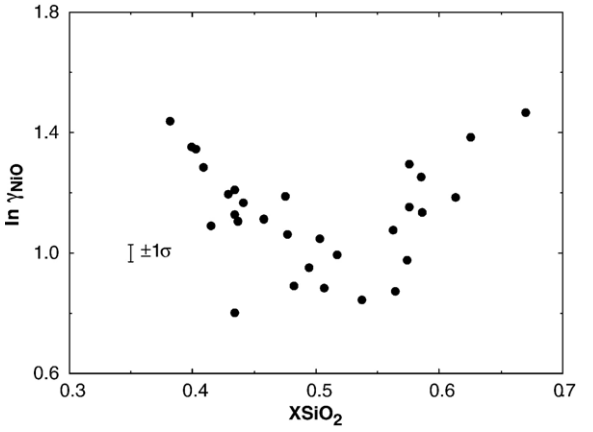

Fig. 3. The relationship between ln γ_{NiO} and X_{SiO_2}, which is approximately parabolic with a minimum at X_{SiO_2}=0.55. Plots of ln γ_{CoO} and ln γ^*_{CrO} versus X_{SiO_2} show a similar shape.

Table 5
Coefficients a_{jk} from fitting γ_{MO} to the subregular solution model for a component at infinite dilution: $\ln\gamma_{MO} = \sum_{j=1}^{4}\sum_{k=1}^{j} a_{jk}X_jX_k$

Ni	X_{Ca}	X_{Mg}	X_{Al}	X_{Si}
X_{Ca}	5.82	13.43	17.43	−8.79
X_{Mg}		2.54	11.01	−5.89
X_{Al}			−6.86	0.50
X_{Si}				4.32
χ^2_ν=3.9, n=30, $\sigma(\gamma_{NiO})$=3%				

Co	X_{Ca}	X_{Mg}	X_{Al}	X_{Si}
X_{Ca}	5.81	12.59	18.47	−12.49
X_{Mg}		2.83	11.77	−9.76
X_{Al}			−6.97	−3.89
X_{Si}				4.40
χ^2_ν=4.3, n=31, $\sigma(\gamma_{CoO})$=3%				

Cr	X_{Ca}	X_{Mg}	X_{Al}	X_{Si}
X_{Ca}	10.47	21.12	17.81	−18.39
X_{Mg}		5.33	11.16	−15.23
X_{Al}			−9.52	−1.65
X_{Si}				4.96
χ^2_ν=3.2, n=29 (L5x omitted), $\sigma(\gamma^*_{CrO})$=5%				

to vary with X_{SiO_2}, but the rule is not hard and fast, and comes with exceptions.

A plot of $\ln \gamma^*_{CrO}/\gamma_{NiO}$ versus optical basicity (Fig. 5b) shows that the data fall within experimental error (except for composition L5x) on two distinct lines, which intersect at an optical basicity value of 0.57. The significance of this is not clear.

4.2. Implications for the thermodynamic modelling of silicate melts

One approach to modelling the thermodynamic properties of silicate melts is the "quasi-crystalline" model, which postulates components that reflect the stoichiometries of the crystals in equilibrium with the melts between their solidi and liquidi (e.g., Burnham, 1981). The idea is that such components mix nearly ideally, when normalised to a constant number of oxygens per formula unit of the component (Burnham suggests 8 oxygens), in contrast to the complex thermodynamic mixing behaviour shown by simple oxide components. For divalent cations, M^{2+}, the component chosen is typically of the form $m(MO{\cdot}nSiO_2)$; e.g., for a quasi-crystalline component with orthosilicate stoichiometry, n=0.5, and if mixing is taken as occurring on 8 oxygen atoms per formula unit, m=4, such that the component is $M_4Si_2O_8$. Because:

$$\mu_{MO\cdot nSiO_2} = \mu_{MO} + n\mu_{SiO_2} \quad (6)$$

and:

$$\mu_{MO} = \mu^o_{MO} + \mathrm{RTln}X_{MO} + \mathrm{RTln}\gamma_{MO} \quad (7)$$

a model with ideal mixing of a $M_4Si_2O_8$ (or similar) component would predict a monotonic inverse correlation between ln γ_{MO} and μ_{SiO_2}, and hence between ln γ_{MO} and X_{SiO_2}, if, as seems reasonable, we assume that μ_{SiO_2} is roughly proportional to X_{SiO_2} for the relatively restricted compositional range of CMAS melts studied here. No such trend is seen (e.g., Fig. 3). The minimum in the plot of ln γ_{MO} with X_{SiO_2} occurs at X_{SiO_2}=0.55, which is not obviously relatable to any particular stoichiometry. While the experimental data reported in this study point to the existence of some fundamental property of CMAS silicate melts that controls the variations of γ_{MO}, we have not been able to identify what this property is.

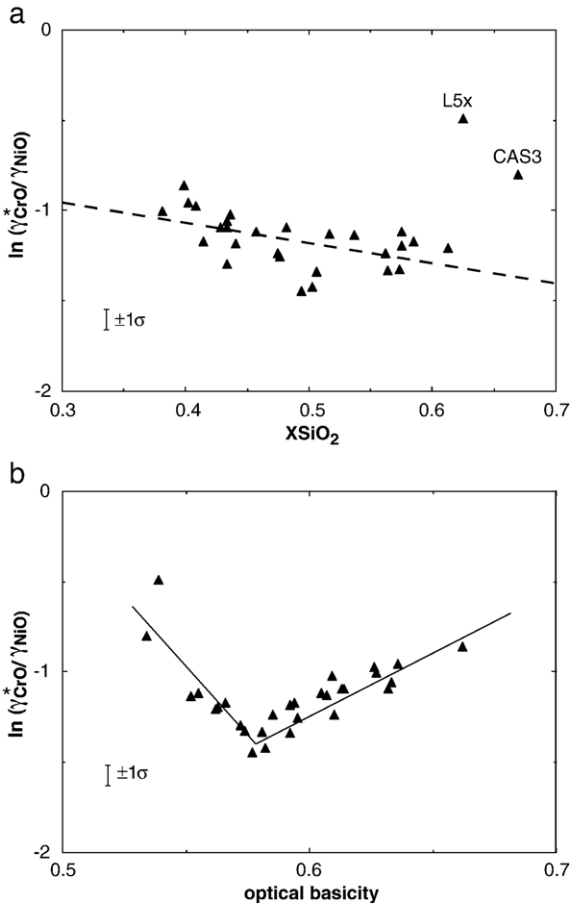

Fig. 5. ln $\gamma^*_{CrO}/\gamma_{NiO}$ versus (a) X_{SiO_2} and (b) optical basicity. The former plot shows a slight negative correlation, indicated by the dashed line, if two high silica compositions (CAS3 and L5x) are omitted from consideration. The latter plot shows that the data appear to fall, within experimental error, on two lines, which intersect at an optical basicity of 0.57.

4.3. Implications for silicate melt structure

There is a set of divalent cations, namely Mg, Mn, Fe, Ni, and Co, that have similar ionic radii and substitute freely for each other in almost all oxide and silicate minerals. We shall refer to these as M^{2+} cations. As an example of the coherent chemical behaviour of this group, consider that each M^{2+} cation forms an orthosilicate, M_2SiO_4, with the olivine crystal structure. Other divalent cations with similar ionic radii such as Cr, Cu and Zn also belong to this group in many circumstances, but show a sufficiently distinctive chemistry to warrant being listed separately. For example, their othosilicates either do not crystallize in the olivine structure (Cr and Zn) or are not known (there are no binary compounds in the system $CuO–SiO_2$). In the case of Cr^{2+}, its distinctive chemistry results from its propensity to occur in highly distorted coordination polyhedra due to the Jahn–Teller effect (as with Cu^{2+}); for Zn (d^{10}), the distinctive chemistry is due to its strong tendency to adopt tetrahedral coordination. Although the importance of the Jahn–Teller effect is well known for Cr^{2+} in "octahedral" crystal sites, it is also strongly developed by Cr^{2+} in tetrahedral coordination, as in the spinel Cr_3O_4 (Li et al., 1995).

This latter point is of special relevance here, as it seems that the preferred coordination environment for M^{2+} cations in aluminosilicate melts is in many cases tetrahedral (see review by Brown et al., 1995). This appears to be the case even for Ni^{2+} (Brown et al., 1995; Farges and Brown, 1996), despite the very large octahedral site preference energy that this cation gets from the crystal field effect (e.g., Burns, 1993, his Table 6.3 on p. 249). Because octahedral coordination for M^{2+} cations is the norm in crystalline silicates, the imposition of tetrahedral symmetry as the preferred coordination environment is presumably due to a geometrical constraint: in a silicate melt in which the M^{2+} cations are surrounded by oxygens that are themselves bonded to Si, accommodating the six M^{2+}–O bonds for octahedral coordination is perhaps difficult for cations of this particular size. This constraint would necessarily apply only to melts that are more siliceous than the orthosilicate composition, in which NBO/T<4 and there are almost no free O^{2-} species (all the composition studied here have NBO/T<2). For highly basic melts with NBO/T>4, which must contain free O^{2-} species, the coordination environment is likely to be similar to that in liquid MO (NBO/T=∞), that is, octahedral, as in the solid MO compounds. That geometrical constraints should force Ni^{2+} into tetrahedral coordination in silicate melts with NBO/T<4 explains the conspicuously higher values of γ_{NiO} compared to those for γ_{CoO} (Table 4) and γ_{FeO} (O'Neill and Eggins, 2002), remembering that the values of γ_{MO} are referred to the standard state of pure liquid MO, in which (presumably) the M^{2+} cations have octahedral coordination.

The correlations among the values of γ_{MO}, where M=Ni, Co and Cr (this study), Fe (O'Neill and Eggins, 2002), and also the major element Mg (Doyle and Naldrett, 1986; Toplis, 2005), are remarkable. In the case of γ_{NiO} and γ_{CoO}, the correlation is as good as the data are precise, which is to ±3% in each. In terms of free energy, this corresponds to ±0.4 kJ mol^{-1} (from $\sigma(\bar{G}_{ex})$= RT$\sigma(\gamma_{MO})/\gamma_{MO}$), which may be compared with the variation in the partial molar free energy, $\bar{G}_{ex}$ (i.e., RTln γ_{MO}) itself of ~10 kJ mol^{-1}, for the range of melts studied here.

Ni^{2+} has a d^8 electronic configuration while Fe^{2+} has d^6 and Co^{2+} d^7, hence the crystal-field stabilization energies of these three cations will differ in different coordination environments. They may also undergo Jahn–Teller distortion to varying degrees, depending on the coordination environment, but it is an empirical observation that the Jahn–Teller effect is much stronger in $Cr^{2+}(d^4)$ than in these other cations (it is also strong in $Cu^{2+}(d^9)$). As regards the Jahn–Teller effect for M^{2+} cations in tetrahedral coordination, it is instructive to consider the chromite spinels, MCr_2O_4, in which the M^{2+} cations are ordered into the tetrahedral site of the spinel structure due to the extremely strong octahedral site preference energy of Cr^{3+}. In this isomorphous series, the cooperative phase transition at which the Jahn–Teller distorted structure transforms to cubic symmetry occurs in $FeCr_2O_4$ at 124 K (Klemme et al., 2000), in $NiCr_2O_4$ at 310 K, but in $CuCr_2O_4$ at 860 K (Inaba et al., 1986). The temperature of the transition in end-member Cr_3O_4 is not known, but from observations in the $MgCr_2O_4$–Cr_3O_4 solid solution it is inferred to persist to very high temperatures (Li et al., 1995). Co^{2+} in tetrahedral coordination is not Jahn–Teller active, nor of course are Mg^{2+} and $Zn^{2+}(d^{10})$. The sequence of strength of the Jahn–Teller effect for M^{2+} cations in tetrahedral coordination is therefore expected to be $Cu^{2+} \cong Cr^{2+} \gg Ni^{2+} > Fe^{2+} > 0 = Co^{2+} = Mg^{2+} = Zn^{2+}$. Note that the difference between octahedral and tetrahedral crystal field stabilization energies (that is, the "octahedral site preference energy" or OSPE) in oxide structures is 86 kJ mol^{-1} for Ni^{2+} but only 31 kJ mol^{-1} for Co^{2+} and 17 kJ mol^{-1} for Fe^{2+} (Burns, 1993) and zero for Mg^{2+} and Zn^{2+}; the differences between these OSPEs are thus very large compared to the ±0.4 kJ mol^{-1} that corresponds to the maximum deviation from the one-to-one correlation between γ_{NiO} and γ_{CoO}.

Given these fundamental differences in electronic structure and resulting chemical behaviour, the correlations between γ_{NiO},γ_{CoO} and γ_{FeO} imply, firstly, that the preferred coordination distributions are much the same for Ni^{2+} as for Co^{2+} and Fe^{2+}; and, secondly, that this preferred coordination distribution does not change with melt composition in the compositional range covered by this study. This second point further implies that there must be sufficient structural freedom for the cations to exist in their preferred coordination distribution regardless of composition. Otherwise the response of each cation to changes in melt composition would surely differ, as it does for Cr^{2+}. The difference in the OSPE between Ni^{2+} and Co^{2+} combined with the exact one-to-one correlation of γ_{NiO} with γ_{CoO} rules out, for example, the hypothesis that the variation of γ_{NiO} (or γ_{CoO}) with composition might be due to a change in the ratio of octahedral to tetrahedral environments in the coordination distribution of the Ni^{2+} (or Co^{2+}) cation.

In summary: the model most consistent with the known chemistry of Ni^{2+}, Co^{2+} and Fe^{2+}, with the various spectroscopic studies of these three cations in glasses and melts, and with the thermodynamic behaviour reported in O'Neill and Eggins (2002) and in this study, is that all three cations have a coordination distribution centred on tetrahedral geometry in CMAS silicate melts. The minor Jahn–Teller distortions expected for Ni^{2+} and Fe^{2+} may be of the dynamic type (Burns, 1993), effectively preserving an averaged tetrahedral symmetry.

We suppose that the different slope for the correlation of γ^*_{CrO} with γ_{NiO} (or γ_{CoO} or γ_{FeO}) is due to the coordination distribution for Cr^{2+} being different to that for Ni^{2+}, Co^{2+}, and Fe^{2+}, because of the strong preference of this d^4 cation for distorted coordination, due to the Jahn–Teller effect. In aqueous solution, complexes of Cr^{2+} in the square-planar configuration (the extreme case of an axially distorted octahedron) are "numerous and stable" (Cotton and Wilkinson, 1988, p. 684), and it is possible that the mean coordination environment of Cr^{2+} in silicate melts represents a compromise between this geometry and the tetrahedral coordination that the melt structure seems more easily to accommodate.

The slope of the correlation of $\ln \gamma^*_{CrO}$ with $\ln \gamma_{MO}$ is itself instructive. The relative changes in γ_{MO} with melt composition are a measure of how easily the melt can accommodate the requirements of the preferred average coordination environment of M^{2+}: high values of γ_{MO} correspond to a relative difficulty with this accommodation, and vice versa. That the slope of the correlation of $\ln \gamma_{CrO}$ with $\ln \gamma_{NiO}$ (and therefore also with $\ln \gamma_{CoO}$ or $\ln \gamma_{FeO}$) is greater than unity (Fig. 2) implies that the difference between two melts in their ability to accommodate Cr^{2+} with its presumed distorted coordination is greater than their difference in ability in accommodating Ni^{2+}; it appears that cations with a preference for distorted coordination may be more sensitive to melt composition than cations preferring a relative symmetrical environment. Nevertheless, the key point of this study is that Cr^{2+} responds to the variations in melt chemistry in the CMAS system in a way that parallels the response of Ni^{2+}, Co^{2+} and Fe^{2+}, which indicates some degree of similarity in coordination environment, but with a systematic difference that makes its behaviour stand out as an anomaly. By contrast, the activity coefficients of a cation like Cr^{3+} that is undoubtedly octahedrally coordinated in silicate melts show no correlation at all with the activity coefficients of the M^{2+} cations (Berry et al., submitted for publication).

Acknowledgements

We thank Dean Scott and Dave Clark for their technical help. The original wireless quench device was designed by Dean, and the drawing of it is by Dave. We acknowledge with pleasure two constructive and informative reviews from Mike Toplis and Hans Keppler, both of whom made several excellent points while allowing us our point of view, even where they may not have completely agreed with the way that we weighed the evidence. We also thank Steve Goldstein for his editorial handling. **[SG]**

References

Berry, A.J., O'Neill, H.St.C., 2004. A XANES determination of the oxidation state of chromium in silicate glasses. Am. Mineral. 89, 790–798.

Berry, A.J., O'Neill, H.St.C., Scott, D.R., Foran, G.F., Shelley, J.M.G., submitted for publication. The effect of composition on Cr^{2+}/Cr^{3+} in silicate melts. Am. Mineral.

Brown, G.E., Fargees, F., Calas, G., 1995. X-ray scattering and X-ray spectroscopy studies of silicate melts. Rev. Miner. 32, 317–410.

Burnham, C.W., 1981. The nature of multicomponent aluminosilicate melts. Phys. Chem. Earth 13, 197–226.

Burns, R.G., 1993. Mineralogical Applications of Crystal Field Theory, 2nd edition. Cambridge University Press, Cambridge, UK.

Calas, G., Cormier, L., Galoisy, L., Jollivet, P., 2002. Structure–property relationships in multicomponent oxide glasses. C. R. Chimie 5, 831–843.

Chase, M.W., 1998. NIST-JANAF thermochemical tables. Journal of Physical and Chemical Reference Data. American Chemical Society, Washington, DC, USA.

Cotton, F.A., Wilkinson, G., 1988. Advanced Inorganic Chemistry, 5th edition. John Wiley, New York.

Doyle, C.D., Naldrett, A.J., 1986. Ideal mixing of divalent cations in mafic magma and its effect on the solution of ferrous oxide. Geochim. Cosmochim. Acta 50, 435–443.

Doyle, C.D., Naldrett, A.J., 1987. Ideal mixing of divalent cations in mafic magma. II. The solution of NiO and the partitioning of nickel between coexisting olivine and liquid. Geochim. Cosmochim. Acta 51, 213–219.

Duffy, J.A., 1993. A review of optical basicity and its applications to oxidic systems. Geochim. Cosmochim. Acta 57, 3961–3970.

Farges, F., Brown, G.E., 1996. An empirical model for the anharmonic analysis of high-temperature XAFS spectra of oxide compounds with applications to the coordination environment of Ni in NiO, γ-Ni_2SiO_4, and Ni-bearing Na-disilicate glass and melt. Chem. Geol. 128, 93–106.

Galoisy, L., Calas, G., 1993. Structural environment of nickel in silicate glass/melt systems: part 1. Spectroscopic determination of coordination states. Geochim. Cosmochim. Acta 57, 3613–3626.

Holzheid, A., O'Neill, H.St.C., 1995. The Cr–Cr_2O_3 oxygen buffer and the free energy of formation of Cr_2O_3 from high-temperature electrochemical measurements. Geochim. Cosmochim. Acta 59, 475–479.

Inaba, H., Yagi, H., Naito, K., 1986. Heat capacity anomalies due to the cooperative Jahn–Teller effect in $Cu_{1-x}Ni_xCr_2O_4$. J. Solid State Chem. 64, 67–75.

Keppler, H., Bagdassarov, N., 1999. The speciation of Ni and Co in silicate melts from optical absorption spectra to 1500 °C. Chem. Geol. 158, 105–115.

Klemme, S., O'Neill, H.St.C., Schnelle, W., Eberhard, G., 2000. The heat capacity of $MgCr_2O_4$, $FeCr_2O_4$, and Cr_2O_3 at low temperatures and derived thermodynamics properties. Am. Mineral. 85, 1686–1693.

Kleykamp, H., 2001. Thermodynamic studies on chromium carbides by the electromotive force (emf) method. J. Alloys Compd. 321, 138–145.

Li, J.-P., O'Neill, H.St.C., Seifert, F., 1995. Subsolidus phase relations in the system MgO–SiO_2–Cr–O in equilibrium with metallic Cr, and their significance for the petrochemistry of chromium J. Petrol. 36, 107–132.

Longhi, J., 1987. Liquidus equilibria and solid solution in the system $CaAl_2Si_2O_8$–Mg_2SiO_4–$CaSiO_3$–SiO_2 at low pressure. Am. J. Sci. 287, 265–331.

Mysen, B.O., 1990. Relationships between silicate melt structure and petrologic processes. Earth Sci. Rev. 27, 281–365.

O'Neill, H.St.C., Eggins, S.M., 2002. An experimental investigation of the effect of melt composition on the activity coefficients of FeO, NiO, CoO, MoO_2 and MoO_3 in silicate melts, and its implications for trace element partitioning. Chem. Geol. 186, 151–181.

Osborn, E.F., Devries, R.C., Gee, K.H., Kraner, H.M., 1954. Optimum composition of blast furnace slag as deduced from liquidus data for the quaternary system CaO–MgO–Al_2O_3–SiO_2. Trans. AIME 200, 33–45.

Pretorius, E.B., Muan, A., 1992. Activity–composition relations of chromous oxide in silicate melts at 1500 °C under strongly reducing conditions. J. Am. Ceram. Soc. 75, 1364–1377.

Rankin, G.A., Wright, F.E., 1915. The ternary system CaO–Al_2O_3–SiO_2. Am. J. Sci. 189, 1–79.

Toker, N.Y., Darken, L.S., Muan, A., 1991. Equilibrium phase relations and thermodynamics for the Cr–O system in the temperature range from 1500° to 1825°C. Metall. Trans. 22B, 225–232.

Schreiber, H.D., 1977. Redox states of Ti, Zr, Hf, Cr, and Eu in basaltic magmas: an experimental study. Proc. Lunar Sci. Conf. 8, 1785–1807.

Toplis, M.J., 2005. The thermodynamics of iron and magnesium partitioning between olivine and liquid: criteria for assessing and predicting equilibrium in natural and experimental systems. Contrib. Mineral. Petrol. 149, 22–39.

Ware, N.G., 1981. Computer programs and calibration with the PIBS technique for quantitative electron probe analysis using a lithium-drifted silicon detector. Comput. Geosci. 7, 167–184.

Xiao, Y., Holappa, L., Reuter, M.A., 2002. Oxidation state and activities of chromium oxides in CaO–SiO_2–CrO_x slag system. Metall. Mater. Trans. 33B, 595–603.